

A method of hard X-ray phase-shifting digital holography

So Yeong Park,^{a*} Chung Ki Hong^a and Jun Lim^b

^aDepartment of Physics, POSTECH, 77 Cheongam-Ro, Pohang, Kyungbuk 37673, South Korea, and ^bBeamline Division, Pohang Light Source, Pohang, Kyungbuk 37673, South Korea. *Correspondence e-mail: soyeongpark@postech.ac.kr

Received 23 December 2015

Accepted 30 May 2016

Edited by A. Momose, Tohoku University, Japan

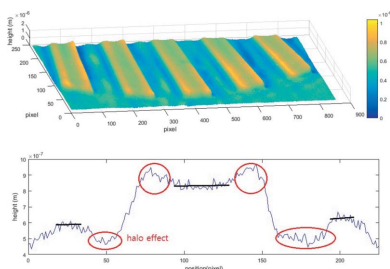
Keywords: X-ray imaging; phase measurement; digital holography; phase-shifting microscopy.

A new method of phase-shifting digital holography is demonstrated in the hard X-ray region. An in-line-type phase-shifting holography setup was installed in a 6.80 keV hard X-ray synchrotron beamline. By placing a phase plate consisting of a hole and a band at the focusing point of a Fresnel lens, the relative phase of the reference and objective beams could be successfully shifted for use with a three-step phase-shift algorithm. The system was verified by measuring the shape of a gold test pattern and a silica sphere.

1. Introduction

Since X-ray radiography was invented by Wilhelm Conrad Röntgen in 1895, X-ray imaging has been a powerful tool for a wide range of research areas from biological to material science, not to mention medical examinations. With transmission X-ray microscopy the inner structure of a specimen can be observed at high resolution owing to the large penetration depth and short wavelength of X-rays. In the case of low-*Z* materials, however, their weak absorption of hard X-rays becomes a problem. Zernike solved the low absorption contrast by introducing a phase difference between the reference wave and the object wave (Zernike, 1955). By inserting a specially designed phase plate at the back focal plane of the objective lens, only the phase of the reference wave is shifted by the phase ring, while the phase of the object wave is not. The phase difference between the two waves enhances the image contrast (Rudolph *et al.*, 1990; Schmahl *et al.*, 1995; Yokosuka *et al.*, 2002; Kagoshima *et al.*, 2002; Neuhäusler *et al.*, 2003; Tkachuk *et al.*, 2007; Chu *et al.*, 2008; Yuan *et al.*, 2012; Chen *et al.*, 2011*a,b*). The resolution of phase-contrast microscopy is, however, degraded by intrinsic halo and shade-off artifacts that arise because part of the object wave also passes through the phase ring. Methods have been proposed to reduce this problem, such as apodization of the phase shifter (Otaki, 2000), the use of an amplitude mask for illumination matched with the phase shifter (Gao *et al.*, 2011), and the use of a beam shaper that defines the illumination with radial dot lines (Vartiainen *et al.*, 2014).

On the other hand, in the visible-light range, phase-shifting digital holography, which can provide quantitative phase images containing much more information than intensity images, has become a very convenient and powerful imaging method (Yamaguchi & Zhang, 1997; Zhang & Yamaguchi, 1998; Kim, 2011). It has been applied to the three-dimensional inspection of microscopic objects with sub-micrometer resolution in biology, microelectronics and microelectromechanical systems engineering. In phase-shifting digital



holography, three or more interference patterns of the reference and the object waves are captured with an electronic image sensor as the phase between the two waves are changed. From the digitally captured interference patterns both the amplitude and the phase distributions of the object field are obtained quantitatively. The amplitude and phase images of the object can be directly obtained in the case of imaging holography, otherwise they can be reconstructed from the object field numerically (Yamaguchi & Zhang, 1997; Zhang & Yamaguchi, 1998; Kim, 2011). The resolution of the phase image can easily be several hundredths of π .

In phase-shifting digital holography, the reference and the object fields, denoted as

$$E_{r,\delta}(x, y) = A_r(x, y) \exp\{i[\theta_r(x, y) - \delta]\} \quad (1)$$

and

$$E_o(x, y) = A_o(x, y) \exp[i\theta_o(x, y)], \quad (2)$$

respectively, are superposed on an electronic detector. In (1) and (2), A and θ are the amplitude and the phase of the waves, respectively, and the subscripts o and r denote the object and the reference waves. (x, y) is the position coordinate and δ is the relative phase-shift introduced to the reference field. The intensity distribution on the detector is then given by

$$I_\delta(x, y) = |E_{r,\delta}(x, y) + E_o(x, y)|^2 \\ = A_r^2(x, y) + A_o^2(x, y) \\ + 2A_r(x, y)A_o(x, y) \cos[\theta_o(x, y) - \theta_r(x, y) + \delta]. \quad (3)$$

In the case of a three-step phase-shifting algorithm with the values of the phase shift δ chosen as $0, \theta$ and $-\theta$, the value of the relative phase between the reference and the object waves is obtained as

$$\theta(x, y) = \theta_o(x, y) - \theta_r(x, y) \\ = \tan^{-1} \left(\frac{I_{-\theta} - I_\theta}{2I_0 - I_{-\theta} - I_\theta} \right). \quad (4)$$

Phase-shifting microscopy has been widely and successfully used in the visible-light range to study the structures of various microscopic samples (Gao *et al.*, 2011; Yamaguchi & Zhang, 1997; Zhang & Yamaguchi, 1998; Kim, 2011). Although there have been various contrast-enhancing methods in X-ray phase

imaging, as listed by Momose (2005), quantitative extraction of the phase maps in the X-ray region has been difficult due to the lack of a precision phase-shifting scheme. Some phase-retrieving schemes have been proposed in the X-ray region such as Fourier transform holography (McNulty *et al.*, 1992; Schlotter *et al.*, 2007), coherent diffraction imaging (Chapman *et al.*, 2006; Miao *et al.*, 2006; Song *et al.*, 2008; Mancuso *et al.*, 2009) and Talbot interferometry (Weitkamp *et al.*, 2005a,b; Pfeiffer *et al.*, 2006), but their results do not show the amount of information and the accuracy of the phase maps that can be obtained with phase-shifting digital holography. Recently some methods of extracting very accurate X-ray maps of samples were developed using interference-fringe-pattern-shifting (Suzuki & Takeuchi, 2014) and phase-shifting X-ray digital holography (Watanabe *et al.*, 2009). In this paper we demonstrate another method of phase-shifting digital holographic microscopy in the hard X-ray region, which combines the phase-shifting mechanism using a specially designed phase plate with modified Zernike phase microscopy.

2. Experimental layout

Fig. 1 shows the optical layout of our experimental setup at the hard X-ray nano-imaging beamline (7C) of the Pohang Light Source (Lim *et al.*, 2013, 2014). A 1.4 m-long hybrid-type in-vacuum undulator with a period of 20 mm (SFA, Korea) is used to generate 6.80 keV X-rays with a 0.182 nm wavelength. The X-rays are monochromated ($\Delta E/E \cong 10^{-4}$) by a Si(111) double-crystal monochromator (DCM; Vactron Korea). A compound refractive lens (CRL) composed of ten beryllium parabolic refractive lenses (RXOPTICS, Germany) with a diameter of 1 mm, which is reduced to an effective aperture of ~ 0.6 mm by absorption, is used as the condenser optics. It is positioned at 25.7 m downstream from the source. At this position, the full width at half-maximum beam size is 2.1 mm \times 0.7 mm. The focal length of the CRL is 3.4 m, and the focused beam size is approximately 70 $\mu\text{m} \times$ 10 μm . The photon flux is estimated as 10^{11} photons s^{-1} from the measurement of the ionization chamber current. In order to homogenize the illumination, a piece of paper is rotated as a diffuser in front of the sample. The sample is mounted on a three-axis piezo-driven scanning stage, which is placed at the center of an air-bearing rotation stage. A 140 μm -diameter

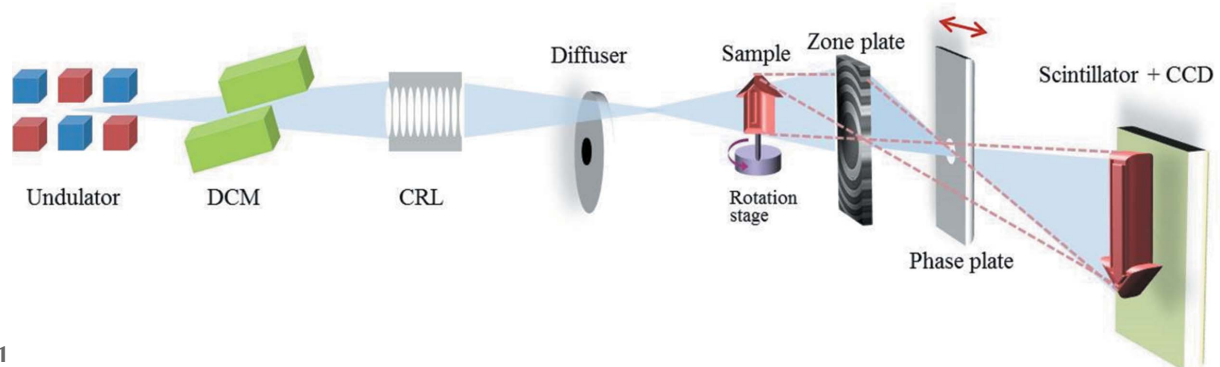


Figure 1
Optical layout of the hard X-ray phase-shifting digital holography setup.

Fresnel zone plate (Zoneplates, UK), which is made of a 1.0 μm -thick tungsten layer and whose outermost zone width, Δr , is 50 nm, is used to focus the image of the sample on the detector plane. The theoretical efficiency of the Fresnel zone plate is $\sim 30\%$ and the first-order focal length is 3.9 cm at 6.80 keV. The X-ray holography setup, shown in Fig. 1, is an off-axis illumination type in which the reference wave, whose beam path is shown in blue, passes through an off-axis region of the Fresnel zone plate. The object wave passes through the whole area of the zone plate and is focused on the detector surface giving the image of the object. The advantage of using such an off-axis illumination geometry is that the reference wave is focused onto a single spot instead of a ring as in typical X-ray phase-contrast imaging schemes. It can, therefore, make the fabrication of the phase plate easier and at the same time reduce the halo effect caused by the part of the object wave that passes through the same area where the phase of the reference wave is controlled (Yokosuka *et al.*, 2002; Kagoshima *et al.*, 2002; Lim *et al.*, 2013, 2014).

The phase-shifting of the relative phase of the reference and the object waves in our system is achieved with the help of a phase plate (Luxel, USA), shown in Fig. 2. It is made from a gold film with a thickness of $685.4 \text{ nm} \pm <7 \text{ nm}$, which increases the phase of the transmitting 6.80 keV X-rays by an additional $\pi/2$. The transmission coefficient of 685.4 nm gold film is about 0.656 at 6.80 keV. The white area of the gold film has been etched out with a focused ion beam. Both the diameter of the hole on the right of Fig. 2(a) and the width of the narrow gold band on the left of Fig. 2(a) are approximately 3 μm , as shown in the electron beam microscopic images of Figs. 2(b) and 2(c). Three areas, each 450 μm square, *i.e.* much larger than the size of the Fresnel zone plate, A1 with a gold band at the center, A2 with just plain gold film, and A3 with a hole at the center, are used for a three-step phase-shifting

algorithm: when the centers of A1, A2 and A3 are placed in turn on the focal plane of the Fresnel zone plate so that the focused reference wave passes through gold, gold and air, respectively, the unfocused object wave passes mainly through air, gold and gold, respectively, and the relative phase-shift in equation (1) becomes $-\pi/2$, 0 and $\pi/2$, respectively. The weakness of our phase plate is that in the case of A1 some part of the object wave passes through the thin band and also the thicker band holding it, which causes a slightly larger halo effect. Although a better phase plate with a hole and a dot instead of a band attached to thicker bands such as in A1 can be fabricated by depositing gold on a certain substrate, it would be more prone to thickness uniformity errors and more costly. Our phase plate guarantees the same magnitude of phase shift for A1 and A3, which outweighs the disadvantage of a larger halo effect.

The position of the phase plate is controlled using ULTRAlign and Gothic Arch XYZ stages (Newport) and picomotor actuators (New Focus). After passing through the phase plate the object wave is focused on the detector plane and the resulting image of the object interferes with the diverged reference wave. A beam stop is placed in front of the detector plane to block the zeroth-order beam so that only the positive first-order beam can form the image, which is made possible by the high magnification of the Fresnel zone plate. The interference patterns are recorded using an online detector consisting of an 18 μm -thick Tb:LSO scintillator coupled to an optical microscope with a 20 \times objective lens and a CCD camera. The CCD camera (U16M; Apogee) has 4096×4096 pixels with an effective pixel size of 0.45 μm and a dynamic range of 16 bits.

3. Hard X-ray phase shifting holography

In conventional phase-shifting microscopy, equation (4) is sufficient to yield the phase information. In our inline phase-shifting digital holography, however, both the intensities and phases of the object and reference waves are changed by the phase plate. Therefore, equation (4) needs to be modified as follows. The zero-phase intensities at the detector plane with and without the gold phase plate inserted are given by

$$I_{0,\text{gold}} = \alpha^2 I_0 = \alpha^2 A_o^2 + \alpha^2 A_r^2 + 2\alpha^2 A_o A_r \cos \theta \quad (5)$$

and

$$I_{0,\text{air}} = I_0 = A_o^2 + A_r^2 + 2A_o A_r \cos \theta, \quad (6)$$

where α is the amplitude transmission coefficient of the gold phase plate. The $-\pi/2$ and $\pi/2$ phase intensities at the detector are given by

$$I_{-\pi/2} = A_o^2 + \alpha^2 A_r^2 + 2\alpha A_o A_r \cos[\theta - (\pi/2)] \quad (7)$$

and

$$I_{\pi/2} = \alpha^2 A_o^2 + A_r^2 + 2\alpha A_o A_r \cos[\theta + (\pi/2)]. \quad (8)$$

The background intensities, which are the intensities without the sample object inserted, are

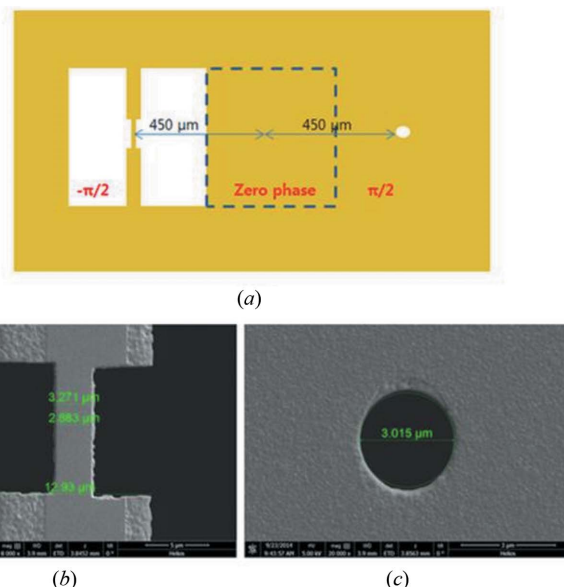


Figure 2 (a) Phase plate made from a gold film for a three-step phase-shifting algorithm. (b, c) Electron beam microscopic images of (a).

$$I_{-\pi/2, \text{bg}} = \alpha^2 A_r^2 \quad (9)$$

and

$$I_{\pi/2, \text{bg}} = A_r^2, \quad (10)$$

when the phases are $-\pi/2$ and $\pi/2$. From (7) to (10), the differences between the intensities with and without the object inserted become

$$I'_{-\pi/2} = I_{-\pi/2} - I_{-\pi/2, \text{bg}} = A_o^2 + 2\alpha A_o A_r \cos[\theta - (\pi/2)] \quad (11)$$

and

$$I'_{\pi/2} = I_{\pi/2} - I_{\pi/2, \text{bg}} = \alpha^2 A_o^2 + 2\alpha A_o A_r \cos[\theta + (\pi/2)]. \quad (12)$$

Then, using (5)–(12) we can obtain

$$\frac{\alpha^2 I'_{-\pi/2} - I'_{\pi/2}}{I_{0, \text{gold}} + I_{0, \text{air}} - I_{\pi/2} - I_{-\pi/2}} = \frac{2\alpha(\alpha^2 + 1)A_o A_r \sin \theta}{2(\alpha^2 + 1)A_o A_r \cos \theta} = \alpha \tan \theta. \quad (13)$$

The value of the relative phase in our inline phase-shifting digital holography system can finally be obtained from

$$\theta = \tan^{-1} \left[\left(\frac{1}{\alpha} \right) \frac{\alpha^2 I'_{-\pi/2} - I'_{\pi/2}}{I_{0, \text{gold}} + I_{0, \text{air}} - I_{\pi/2} - I_{-\pi/2}} \right]. \quad (14)$$

The transmission coefficient, α , of our gold phase plate is 0.809.

4. Result

We have verified the feasibility of the proposed setup by measuring samples with known dimensions: a Siemens star test pattern made of gold (Xradia, X-30-30-2) with a thickness of $200 \text{ nm} \pm 10\%$ and a $1.5 \text{ }\mu\text{m}$ -diameter silica sphere. Fig. 3 shows the interference images of the test pattern obtained as the relative phase shifted: (a) with 0 phase shift, (b) and (c) with phase shifts of $-\pi/2$ and $\pi/2$, respectively. The thickness of the sample can be found by using the relationship between the phase and the refractive index of a material, $\Phi = 2\pi d \Delta n / \lambda$, where d is the thickness of the material, Δn is the refractive index of the material (6.44×10^{-5} for Au at 6.80 keV), and λ is the wavelength (0.182 nm at 6.80 keV). The three-dimensional plot of the measured thickness of the gold test pattern is shown in Fig. 4(a). The height profile of the test pattern on the red line in Fig. 3(a) is shown in Fig. 4(b). The red circles depict the area of the halo and show that our system requires improvement. The thickness of the gold pattern is obtained from the difference between the height of the top and bottom horizontal lines as $219 \pm 18 \text{ nm}$.

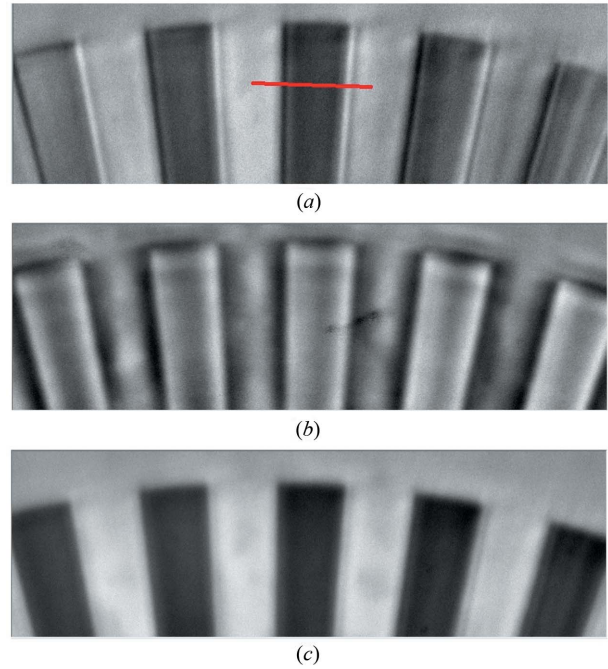


Figure 3 Hard X-ray images of a gold Siemens star pattern formed by the interference between the reference wave and object waves for three different relative phases: (a) zero, (b) $-\pi/2$ and (c) $\pi/2$.

The accuracy of about 18 nm is estimated from the standard deviation of the phase fluctuation at the central flat region of the phase image. The edge of sample was affected by the halo effect of the Zernike phase-contrast method. For this reason, we excluded the data of the halo region. The thickness test pattern which includes the halo region is $238 \pm 34 \text{ nm}$. According to the sample, the amplitude of the reference waves

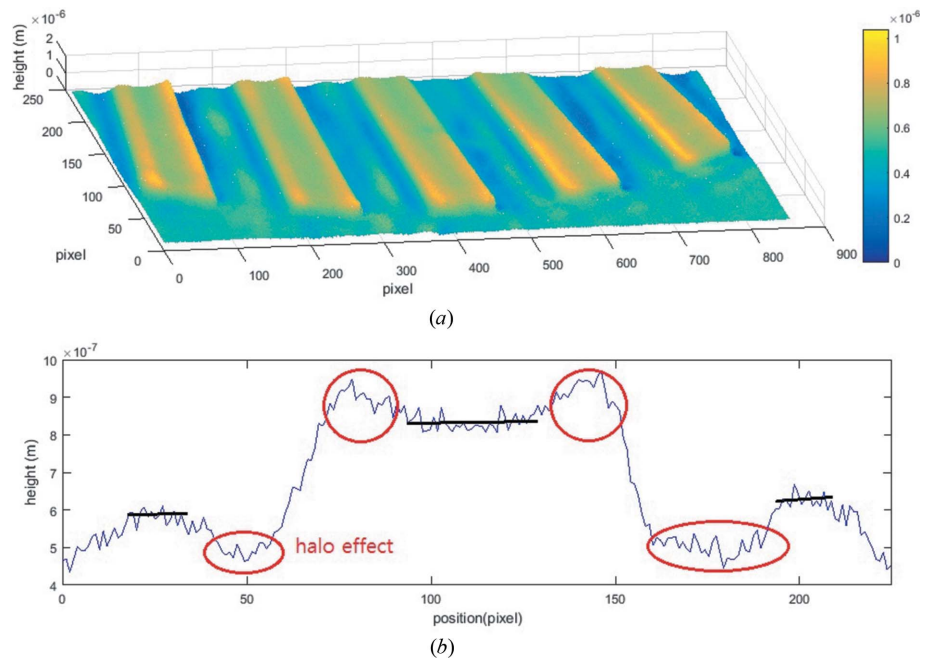


Figure 4 (a) Three-dimensional plot of the phase image and (b) the thickness line profile of a gold test pattern with a nominal thickness of 200 nm.

in equations (7)–(10) are different due to absorption in the sample. The transmittance of the 200 nm gold test pattern is about 0.884. In equations (11)–(12), we subtract background reference waves from the $-\pi/2$ and $\pi/2$ phase intensities. To avoid the error from the difference between background reference waves and reference waves of the $-\pi/2$ and $\pi/2$ phase in equations (11)–(12), we multiply the transmission rate 0.884 by the background wave equations (9)–(10). The experimental result before the error correction is 228 ± 18 nm. The nominal thickness, 200 ± 20 nm, of the Au test pattern supplied by the manufacturer is slightly different from our measurement result. The difference between the two values is assumed to be due to the halo effect appearing in typical Zernike phase-contrast microscopy, which can be reduced by improving the phase plate, and needs further investigation. Fig. 5 shows the interference images of a silica sphere with a nominal diameter of $1.5 \mu\text{m}$ obtained with three different relative phases between the reference and the object wave. Although the sample is a sphere, the plot shows only the accumulated phase delays along the X-ray propagation direction. The true structure of the sample can be obtained only from a tomographical measurement. The thickness is obtained by applying $\Phi = 2\pi d\Delta n/\lambda$ with $\Delta n = 1.059 \times 10^{-5}$ for SiO_2 at $\lambda = 0.182$ nm. The thickness profile on the red line in Fig. 5(a) is shown in Fig. 6(b). The diameter of the silica sphere is found to be $1.62 \pm 0.13 \mu\text{m}$ from the distance between the two horizontal marked in Fig. 6(b). This result is in good agreement with the value of $1.5 \mu\text{m}$ supplied by the manufacturer.

5. Conclusion

In conclusion, we have demonstrated a new method of phase-shifting digital holography in hard X-ray microscopy by combining Zernike phase-contrast microscopy with three-step phase-shifting digital holography. The use of an off-axis illumination scheme of X-ray transmission microscopy together with a specially designed phase plate for a three-step phase-shifting algorithm of digital holography made it possible to obtain quantitative phase images in addition to the usual intensity images of the samples. The thickness of a gold test pattern and the diameter of a silica sphere were measured

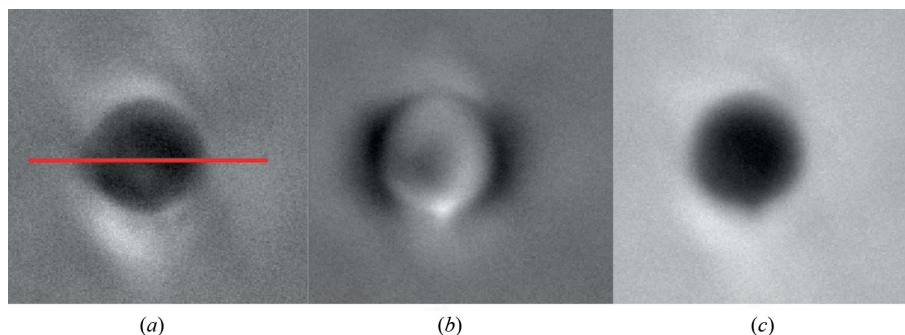


Figure 5 X-ray images of a $1.5 \mu\text{m}$ silica sphere formed by the interference between the reference wave and object waves for three different relative phases: (a) zero, (b) $-\pi/2$ and (c) $\pi/2$.

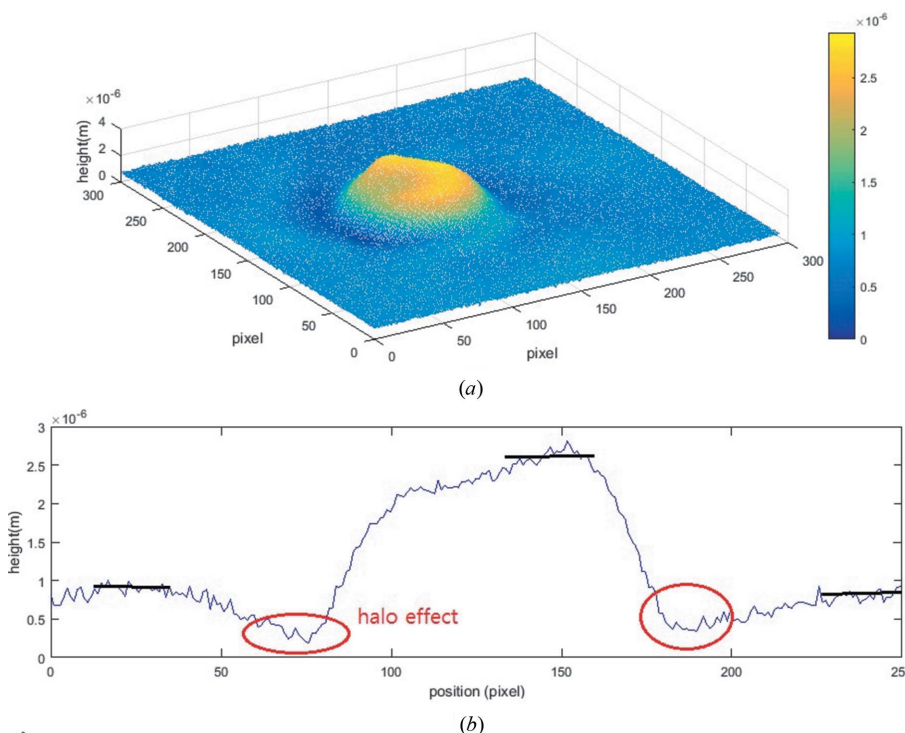


Figure 6 (a) Three-dimensional plot of the phase image and (b) a thickness line profile of a $1.5 \mu\text{m}$ silica sphere.

using our setup. Although the results were in good agreement with the nominal values, the phase images still showed halo effects, which were inherent to the phase-contrast X-ray imaging method that causes some phase errors.

Acknowledgements

This work was financially supported by the National Research Foundation of Korea (NRF) as a grant funded by the Korean government (NRF-2013M2A2A9046502).

References

Chapman, H. N., Barty, A., Bogan, M. J., Boutet, S., Frank, M., Hauser, S. P., Marchesini, S., Woods, B. W., Bajt, S., Benner, W. H., London, R. A., Plönjes, E., Kuhlmann, M., Treusch, R., Düsterer, S., Tschentscher, T., Schneider, J. R., Spiller, E., Möller, T., Bostedt,

- C., Hoener, M., Shapiro, D. A., Hodgson, K. O., van der Spoel, D., Burmeister, F., Bergh, M., Coleman, C., Huldt, G., Seibert, M. M., Maia, F. R. N. C., Lee, R. W., Szöke, A., Timneanu, N. & Hajdu, J. (2006). *Nat. Phys.* **2**, 839–843.
- Chen, T. Y., Chen, Y. T., Wang, C. L., Kempson, I. M., Lee, W. K., Chu, Y. S., Hwu, Y. & Margaritondo, G. (2011a). *Opt. Express*, **19**, 19919–19924.
- Chen, Y. T., Chen, T. Y., Yi, J., Chu, Y. S., Lee, W. K., Wang, C. L., Kempson, I. M., Hwu, Y., Gajdosik, V. & Margaritondo, G. (2011b). *Opt. Lett.* **36**, 1269–1271.
- Chu, Y. S., Yi, J. M., De Carlo, F., Shen, Q., Lee, W. K., Wu, H. J., Wang, C. L., Wang, J. Y., Liu, C. J., Wang, C. H., Wu, S. R., Chien, C. C., Hwu, Y., Tkachuk, A., Yun, W., Feser, M., Liang, K. S., Yang, C. S., Je, J. H. & Margaritondo, G. (2008). *Appl. Phys. Lett.* **92**, 103119.
- Gao, P., Yao, B., Harder, I., Lindlein, N. & Torcal-Milla, F. J. (2011). *Opt. Lett.* **36**, 4305–4307.
- Kagoshima, Y., Yokoyama, Y., Ibuki, T., Niimi, T., Tsusaka, Y., Takai, K. & Matsui, J. (2002). *J. Synchrotron Rad.* **9**, 132–135.
- Kim, M. K. (2011). *Digital Holographic Microscopy: Principles, Techniques, and Applications*. New York: Springer.
- Lim, J., Kim, H. & Park, S. Y. (2014). *J. Synchrotron Rad.* **21**, 827–831.
- Lim, J., Park, S. Y., Huang, J. Y., Han, S. M. & Kim, H. T. (2013). *Rev. Sci. Instrum.* **84**, 013707.
- Mancuso, A. P., Schropp, A., Reime, B., Stadler, L.-M., Singer, A., Gulden, J., Streit-Nierobisch, S., Gutt, C., Grübel, G., Feldhaus, J., Staier, F., Barth, R., Rosenhahn, A., Grunze, M., Nisius, T., Wilhein, T., Stickler, D., Stillrich, H., Frömter, R., Oepen, H.-P., Martins, M., Pfau, B., Günther, C. M., Könecke, R., Eisebitt, S., Faatz, B., Guerassimova, N., Honkavaara, K., Kocharyan, V., Treusch, R., Saldin, E., Schreiber, S., Schneidmiller, E. A., Yurkov, M. V., Weckert, E. & Vartanyants, I. A. (2009). *Phys. Rev. Lett.* **102**, 035502.
- McNulty, I., Kirz, J., Jacobsen, C., Anderson, E. H., Howells, M. R. & Kern, D. P. (1992). *Science*, **256**, 1009–1012.
- Miao, J., Chen, C. C., Song, C., Nishino, Y., Kohmura, Y., Ishikawa, T., Ramunno-Johnson, D., Lee, T. K. & Risbud, S. H. (2006). *Phys. Rev. Lett.* **97**, 215503.
- Momose, A. (2005). *Jpn. J. Appl. Phys.* **44**, 6355–6367.
- Neuhäusler, U., Schneider, G., Ludwig, W., Meyer, M. A., Zschech, E. & Hambach, D. (2003). *J. Phys. D*, **36**, A79–A82.
- Otaki, T. (2000). *Opt. Rev.* **7**, 119–122.
- Pfeiffer, F., Weitkamp, T., Bunk, O. & David, C. (2006). *Nat. Phys.* **2**, 258–261.
- Rudolph, D., Schmahl, G. & Niemann, B. (1990). *Modern Microscopies, Techniques and Applications*, edited by P. J. Duke and A. G. Michette, pp. 59–67. New York: Plenum.
- Schlottter, W. F., Lüning, J., Rick, R., Chen, K., Scherz, A., Eisebitt, S., Günther, C. M., Eberhardt, W., Hellwig, O. & Stöhr, J. (2007). *Opt. Lett.* **32**, 3110–3112.
- Schmahl, G., Rudolph, D., Guttman, P., Schneider, G., Thieme, J. & Niemann, B. (1995). *Rev. Sci. Instrum.* **66**, 1282–1286.
- Song, C., Jiang, H., Mancuso, A., Amirbekian, B., Peng, L., Sun, R., Shah, S. S., Zhou, Z. H., Ishikawa, T. & Miao, J. (2008). *Phys. Rev. Lett.* **101**, 158101.
- Suzuki, Y. & Takeuchi, A. (2014). *Jpn. J. Appl. Phys.* **53**, 122501.
- Tkachuk, A., Duerwer, F., Cui, H., Feser, M., Wang, S. & Yun, W. (2007). *Z. Kristallogr.* **222**, 650–655.
- Vartiainen, I., Mokso, R., Stampanoni, M. & David, C. (2014). *Opt. Lett.* **39**, 1601–1604.
- Watanabe, N., Hoshino, M., Yamamoto, K., Aoki, S., Takeuchi, A. & Suzuki, Y. (2009). *J. Phys. Conf. Ser.* **186**, 012021.
- Weitkamp, T., Diaz, A., David, C., Pfeiffer, F., Stampanoni, M., Cloetens, P. & Ziegler, E. (2005a). *Opt. Express*, **13**, 6296–6304.
- Weitkamp, T., Nöhammer, B., Diaz, A., David, C. & Ziegler, E. (2005b). *Appl. Phys. Lett.* **86**, 054101.
- Yamaguchi, I. & Zhang, T. (1997). *Opt. Lett.* **22**, 1268–1270.
- Yokosuka, H., Watanabe, N., Ohigashi, T., Yoshida, Y., Maeda, S., Aoki, S., Suzuki, Y., Takeuchi, A. & Takano, H. (2002). *J. Synchrotron Rad.* **9**, 179–181.
- Yuan, Q., Zhang, K., Hong, Y., Huang, W., Gao, K., Wang, Z., Zhu, P., Gelb, J., Tkachuk, A., Hornberger, B., Feser, M., Yun, W. & Wu, Z. (2012). *J. Synchrotron Rad.* **19**, 1021–1028.
- Zernike, F. (1955). *Science*, **121**, 345–349.
- Zhang, T. & Yamaguchi, I. (1998). *Opt. Lett.* **23**, 1221–1223.